

A Human Ribonuclease Variant and ERK-Pathway Inhibitors Exhibit Highly Synergistic Toxicity for Cancer Cells

Trish T. Hoang¹, I. Caglar Tanrikulu^{1,2}, Quinn A. Vatland¹, Trieu M. Hoang¹, and Ronald T. Raines^{1,2,3}



Abstract

Pancreatic-type ribonucleases (ptRNases) are prevalent secretory enzymes that catalyze the cleavage of RNA. Ribonuclease inhibitor (RI) is a cytosolic protein that has femtomolar affinity for ptRNases, affording protection from the toxic catalytic activity of ptRNases, which can invade human cells. A human ptRNase variant that is resistant to inhibition by RI is a cytotoxin that is undergoing a clinical trial as a cancer chemotherapeutic agent. We find that the ptRNase and protein kinases in the ERK pathway exhibit

strongly synergistic toxicity toward lung cancer cells (including a KRAS^{G12C} variant) and melanoma cells (including BRAF^{V600E} variants). The synergism arises from inhibiting the phosphorylation of RI and thereby diminishing its affinity for the ptRNase. These findings link seemingly unrelated cellular processes, and suggest that the use of a kinase inhibitor to unleash a cytotoxic enzyme could lead to beneficial manifestations in the clinic. *Mol Cancer Ther*; 17(12); 2622–32. ©2018 AACR.

Introduction

As catalysts of RNA degradation, ribonucleases operate at the crossroads of transcription and translation. This central role is suggestive of potential clinical utility. Indeed, experiments in the 1950s showed that RNase A, which is a secretory pancreatic-type ribonuclease (ptRNase), was toxic to tumor cells, both *in vitro* and *in vivo* (1–3). Efficacy required, however, the injection of a large quantity (i.e., milligrams) of enzyme into a solid tumor.

In recent years, the need for high dosing was overcome with variants of RNase A that evade ribonuclease inhibitor (RI), a protein that is endogenous to the cytosol of human cells (4–6). Moreover, RNase A was found to have an innate affinity for Globo H, which is a tumor-associated antigen (7). These discoveries have led to the development of RI-evasive variants of RNase 1 (which is a human homolog of RNase A) as cancer chemotherapeutic agents. One such variant, QBI-139, is in a phase I clinical trial for the treatment of solid tumors (8, 9).

The combination of drugs can be of substantial benefit to patients with cancer (10, 11). In a study of solid tumors, Nowak, Vogelstein, and their coworkers have shown that, in most clinical cases, combination therapies will be needed to avoid the evolution of resistance to targeted drugs (12). In addition to therapeutic

advantages, combination therapy can provide significant long-term cost savings to patients and society compared with the use of single agents. QBI-139 has no particular "target" other than cellular RNA and is thus unlikely to engender resistance. Still, we imagined that mutual benefit might arise from its pairing with extant cancer drugs.

Small-molecule inhibitors of protein kinases, especially in combination with other drugs, are playing an increasingly prominent role in the treatment of cancer (13). The focus on kinases derives from their central role in regulating cellular processes (14, 15). For example, aberrant protein phosphorylation in the ERK pathway (i.e., RAS–RAF–MEK–ERK) is known to promote the development and progression of cancer. Accordingly, kinases of the ERK pathway are the target of many drugs (16, 17). The acquisition of resistance to these drugs as stand-alone therapies is, however, common (18, 19).

Herein, we probe the efficacy of combining a human ribonuclease variant, QBI-139, with small-molecule kinase inhibitors as toxins for human cancer cells. We discover *remarkable* synergism with agents that target the ERK pathway. This synergism greatly exceeds that from merely pairing kinase inhibitors. We find that the biochemical basis for the synergism of a ribonuclease and a kinase inhibitor entails the previously unknown phosphorylation of RI. These findings reveal a link between previously unrelated cellular processes, and could lead to beneficial manifestations in the clinic.

Materials and Methods

Materials

All chemicals were from Sigma–Aldrich, Invitrogen, or Thermo Fisher Scientific unless indicated otherwise, and were used without further purification. All primary antibodies were from Cell Signaling Technology. All secondary antibodies were from Santa Cruz Biotechnologies. QBI-139 was a kind gift from Dr. L.E. Strong (Quintessence Biosciences, Madison, WI). All

¹Department of Biochemistry, University of Wisconsin–Madison, Madison, Wisconsin. ²Department of Chemistry, Massachusetts Institute of Technology, Cambridge, Massachusetts. ³Department of Chemistry, University of Wisconsin–Madison, Madison, Wisconsin.

Note: Supplementary data for this article are available at Molecular Cancer Therapeutics Online (<http://mct.aacrjournals.org/>).

Corresponding Author: Ronald T. Raines, Massachusetts Institute of Technology, 77 Massachusetts Avenue, Cambridge, Massachusetts 02139. Phone: 617-253-1470; E-mail: rraines@mit.edu

doi: 10.1158/1535-7163.MCT-18-0724

©2018 American Association for Cancer Research.

kinase inhibitors were from Selleckchem. Aqueous solutions were made with water that was generated with an Atrium Pro water purification system from Sartorius and had resistivity $\geq 18 \text{ M}\Omega\cdot\text{cm}^{-1}$. Procedures were performed at room temperature ($\sim 22^\circ\text{C}$) unless indicated otherwise.

Cell culture

Human cells were obtained from the ATCC and stored in vials immersed in $\text{N}_2(\text{l})$. Before their use, human cell lines were authenticated by morphology, karyotyping, and PCR-based methods, which included an assay to detect species specific variants of the cytochrome C oxidase I gene (to rule out inter-species contamination) and short tandem repeat profiling (to distinguish between individual human cell lines and rule out intraspecies contamination). To minimize genetic drift, a thawed vial was used for fewer than fifteen passages.

Medium and added components, trypsin (0.25% w/v), and Dulbecco's PBS were from the Gibco brand from Thermo Fisher Scientific. Cells were grown in flat-bottomed culture flasks in a cell-culture incubator at 37°C under $\text{CO}_2(\text{g}; 5\% \text{ v/v})$. A549 cells (ATCC CCL-185) were grown in F-12K medium; H358 (ATCC CRL-5807) cells were grown in RPMI-1640 medium; SK-MEL-28 cells (ATCC HTB-72) were grown in Eagle's minimum essential medium; A375 cells (ATCC CRL-1619) and HEK293T cells (ATCC CRL-1573) were grown in Dulbecco's modified Eagle's medium; Malme-3M (ATCC HBT-64) cells were grown in Iscove's modified Dulbecco's medium; Malme-3 (ATCC HTB-102) cells were grown in McCoy's 5a modified medium. The Corning 96-well microplates used in experiments were from Sigma-Aldrich.

Assay of cell viability with a single drug

Assays for cell viability in the presence of a drug(s) were performed with a tetrazolium dye-based assay for cellular metabolic activity (20). Cells in complete growth medium were plated at 5,000 cells per well in a 96-well microplate, which was incubated for 24 hours. Cells were then treated with increasing concentrations of each compound, either kinase inhibitors or QBI-139. After 48 hours, the medium was removed, and cells were incubated for 2 hours with CellTiter 96 MTS reagent from Promega. Absorbance was recorded on an M1000 fluorimeter from Tecan at 490 nm. Data were analyzed with Prism 5.0 software from GraphPad. Values of EC_{50} , which is the concentration of a drug that gives half-maximal cell viability, were calculated with the equation:

$$\gamma = \gamma_{\min} + \frac{\gamma_{\max} - \gamma_{\min}}{1 + 10^{(\log EC_{50} - x)h}},$$

where γ is cell viability, x is the concentration of drug, and h is the Hill coefficient. Data were plotted on a log scale with each data point being the mean of 3 biological replicates.

Assay of cell viability with two drugs

The EC_{50} values obtained from single-drug cell viability assays were used to design subsequent drug combination experiments. Two-drug combination experiments were performed by using a 5×5 matrix in 96-well plates to interrogate 25 dosing pairs. Cells in complete growth medium were plated at 5,000 cells per well in a 96-well microplate, which was incubated for 24 hours at 37°C . Cells were treated with kinase inhibitor for 1 hour, followed by QBI-139. After 48 hours, cell viability was evaluated as described above.

Dose-response data for each drug alone and for two-drug combinations were determined experimentally. CI values were calculated using CalcuSyn 2.0 from Biosoft. $CI < 1$, $CI = 1$, and $CI > 1$ indicate synergism, an additive effect, and antagonism, respectively. Each CI value was the mean of data from 3 biological replicates.

Cloning of genes encoding BAP-RI and BirA

A DNA fragment encoding human wild-type RI was a generous gift from Promega. DNA primers encoding BAP and a linker peptide, GSGSGS, were installed on the N terminus of RI by amplification using PCR. The PCR-amplified gene encoding the BAP-RI conjugate was inserted into pNeo3 vector by using Gibson assembly (21). A DNA fragment encoding BirA was a kind gift from Prof. M. Wickens (University of Wisconsin-Madison). The gene was inserted into pNeo3 vector by using Gibson assembly (21). The sequences of the BAP-RI and BirA constructs were confirmed by DNA sequencing at the University of Wisconsin Biotechnology Center.

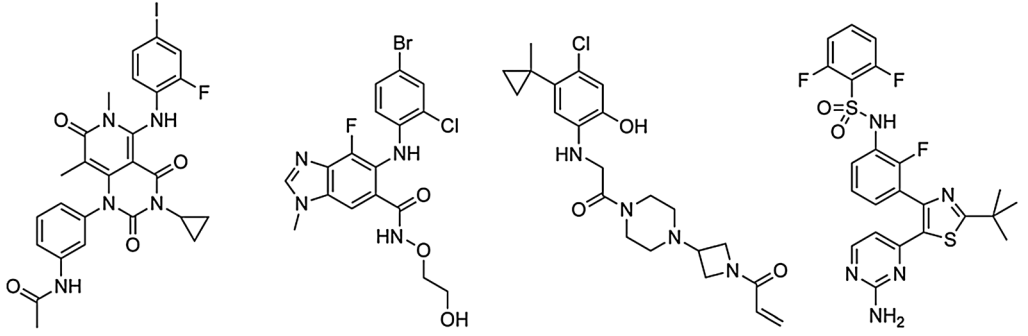
Expression and purification of biotinylated RI

HEK293T cells were seeded in complete medium in 6-well plates or 10-cm dishes at a density of 200 cells/ μL . After 24 hours, cells were transfected with plasmids that direct the expression of BirA and BAP-RI using Lipofectamine 3000. One hour later, biotin (1 $\mu\text{mol/L}$) was added into transfected cells, and incubation was continued for another 48 hours. Cells were harvested, washed with PBS, and then lysed in lysis buffer (which was M-PER Mammalian Protein Extraction Reagent containing Pierce Protease Inhibitor Tablets, Pierce Phosphatase Inhibitor Tablets, and 1 mmol/L DTT). Cell lysate was subjected to centrifugation at 14,000g for 30 minutes at 4°C to remove cell debris. The clarified lysate was filtered, and then applied to monomeric avidin-agarose beads. The mixture was subjected to nutation for 24 hours at 4°C . The beads were washed ($3\times$) with lysis buffer, and then eluted with lysis buffer containing 2 mmol/L biotin. The eluate was then purified further by chromatography using a 5-mL ribonuclease A-affinity column as described previously (22). The purified, biotinylated RI was stored in storage buffer (which was 20 mmol/L Tris-HCl buffer, pH 7.5, containing 1 mmol/L EDTA, 1 mmol/L DTT, and 50 mmol/L NaCl). The protein sample was then submitted to mass spectrometry at University of Wisconsin Biotechnology Center to identify any sites of phosphorylation.

Immunoblotting

Immunoblotting was performed by standard methods, as described previously (23). Cells grown in a 10-cm dish were lysed with 1 mL of M-PER Mammalian Protein Extraction Reagent containing Pierce Protease Inhibitor Tablets, Pierce Phosphatase Inhibitor Tablets, and DTT (1 mmol/L). Cell lysates were subjected to centrifugation for 10 minutes at $14,000 \times g$ to remove cell debris, and the total protein concentration in the supernatant was determined with a Bradford protein assay. Protein ($\sim 30 \mu\text{g}$) was separated by SDS-PAGE using a gel from Bio-Rad, and the resulting gel was subjected to transfer to a PVDF membrane with an iBlot 2 dry transfer system. The membrane was blocked for 1 hour in a solution of BSA (5% w/v) in TBS-Tween (TBS-T), washed, and then incubated overnight at 4°C with an antibody (1:500 dilution) in TBS-T containing BSA (5% w/v). After another wash with

Table 1. Toxicity of agents for human lung cancer cells (A549)

			
Trametinib	Selumetinib	ARS-853	Dabrafenib
Agent	Kinase target	EC ₅₀ (μmol/L) ^a	Synergism with QBI-139?
Kinase inhibitor (non-ERK pathway)			
PD 0332991	Cdk4 and Cdk5	0.24 ± 0.04	No
Bosutinib	c-Src and Abl	0.73 ± 0.06	No
Crizotinib	c-MET and ALK	0.11 ± 0.02	No
Kinase inhibitor (ERK pathway)			
Trametinib	MEK1/2	5.7 ± 0.6	Yes
Selumetinib	MEK1/2	43 ± 5	Yes
ARS-853	KRAS ^{G12C}	74 ± 8	Yes
Dabrafenib	BRAF ^{V600E}	40 ± 5	Yes
ptRNase			
QBI-139	(RNA)	62 ± 7	—

^aValues (±SE) are for cell viability as measured with a tetrazolium dye-based assay for metabolic activity (*n* = 3, biological replicates).

TBS-T, membranes were incubated with secondary antibody (1:3,000 dilution), washed again, and then detected with an Amersham ECL Select Western Blotting Detection Reagent and by an ImageQuant LAS4000 instrument from GE Healthcare.

For pull-down assays, after isolation of the total protein, samples were incubated overnight at 4°C with Streptavidin MagneSphere Paramagnetic Particles from Promega. The beads were washed (3×) with PBS containing 1 mmol/L DTT. Samples were eluted with 50 μL of SDS gel-loading dye and processed further for immunoblotting.

Native gel-shift assay

RI purified from transfected HEK293T cells was subjected to electrophoresis through a non-denaturing gel in the absence and presence of QBI-139, as described previously (24). Unphosphorylated RI (uRI; 3 μmol/L) was prepared by incubating isolated RI with lambda protein phosphatase from New England BioLabs (Ipswich, MA) for 10 minutes at 37°C, followed by dialysis against PBS containing 1 mmol/L DTT to remove excess phosphatase. RI (or uRI) and QBI-139 were incubated together in a 1:1.3 or 1:1 molar ratio for 20 minutes at 25°C to allow for complex formation. A 10-μL aliquot of protein solution was combined with 2 μL of a 6 × solution of SDS gel-loading dye, and the resulting mixtures were applied immediately onto a non-denaturing 12% w/v polyacrylamide gel from Bio-Rad. Gels were subjected to electrophoresis in the absence of SDS at 20 to 25 mA for approximately 3 hours at 4°C and stained with Coomassie Brilliant Blue G-250 dye.

Protein thermal-shift assay

Values of *T_m* for RI in the absence and presence of QBI-139 were determined with differential scanning fluorimetry (DSF;

ref. 25). DSF was performed with a ViiA 7 Real-Time PCR machine from Applied Biosystems. Briefly, a 20-μL solution of protein (10 μmol/L of RI or uRI; 14 μmol/L of QBI-139) was loaded into the wells of MicroAmp optical 96-well plate from Applied Biosystems, and SYPRO Orange dye was added to a final dilution of 1:250 in relation to the stock solution from the manufacturer. The temperature was increased from 20°C to 96°C at 1°C/min in steps of 1°C. Fluorescence intensity was measured at 578 nm, and the denaturation curve was fitted with Protein Thermal Shift software from Applied Biosystems to determine values of *T_m*, which is the temperature at the midpoint of the transition.

Calculation of Coulombic interaction energies

Calculations were performed on AMD Opteron 2.2-GHz processors running CentOS 6.3 at the Materials and Process Simulation Center of the California Institute of Technology (Pasadena, CA). All computational models were based on the crystal structure of the human RI-RNase 1 complex (PDB entry 1z7x), which was determined at a resolution of 1.95 Å (22). Missing hydrogen atoms were introduced with the program Reduce (version 3.03), and the model was minimized fully (26). All minimizations were carried out to a 0.2 kcal/mol/Å RMS-force convergence criterion by conjugate gradient minimization in vacuum using the DREIDING force-field (27, 28).

The Coulombic impact of replacing Ser/Thr residues with pSer/pThr on the stability of the RI-RNase 1 complex was calculated as the difference between the energy of the complex and that of its components. Serine and threonine residues at phosphorylation sites were replaced with glutamine, and side-chain conformations of these and other residues within 6 Å were optimized with the

program SCREAM (29). Following minimization, glutamine side-chains were replaced with pSer or pThr with purpose-written Python (version 2.7) scripts, and the phosphorylated complex was minimized locally. All Coulombic interaction energies reported are relative to that calculated for the wild-type complex.

Similarly, the Coulombic impact of phosphorylation on thiolate formation at cysteine side-chains of RI was calculated through the change in Coulombic interaction energy between a cysteine thiolate and RI upon phosphorylation at a specific site.

Results

A kinase inhibitor enhances the cytotoxicity of a pTrNase

In an initial screen, we treated human lung cancer cells (line A549) for 48 hours with four inhibitors of four different types of protein kinases: trametinib, PD 0332991, bosutinib, and crizotinib (30–32). We measured cell viability with a tetrazolium dye-based assay for metabolic activity. The ensuing EC_{50} values are listed in Table 1. Next, we treated cells with kinase inhibitors at their EC_{50} concentrations for 1 hour before the addition of QBI-139 (10 μ mol/L), and assessed cell viability after 48 hours. We found that treatment with trametinib in combination with QBI-139 was more effective at killing lung cancer cells than was treatment with either agent by itself (Fig. 1). In contrast, combinations of QBI-139 with other kinase inhibitors resulted in cytotoxicity comparable with that with the kinase inhibitor alone.

MEK inhibitors act synergistically with a pTrNase

To investigate possible synergy between QBI-139 as well as another MEK inhibitor, selumetinib, we evaluated a range of drug combinations. First, we characterized the cytotoxicity of single-drug treatments in the A549 cell line (Fig. 2A). We used the EC_{50} values obtained from single-drug treatments (Table 1) to design subsequent drug combination experiments. Two-drug combination experiments were performed using a 5×5 matrix to interrogate 25 dosing pairs per combination. Each drug was dosed at five concentrations obtained by serial two-fold dilutions. We

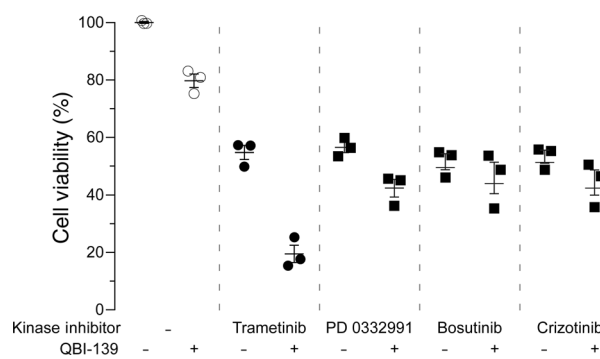


Figure 1.

An ERK-pathway inhibitor enhances the toxicity of a ribonuclease toward human lung cancer cells. A549 cells were treated with kinase inhibitors at their EC_{50} concentrations (Table 1) for 1 hour before the addition of QBI-139 (10 μ mol/L) or vehicle. Cell viability was assessed after another 48 hours. Treatment with trametinib combined with QBI-139 is highly effective at killing lung cancer cells. Combinations of QBI-139 with other kinase inhibitors result in toxicity similar to that from the kinase inhibitor alone. Values represent the mean \pm SEM ($n = 3$, biological replicates).

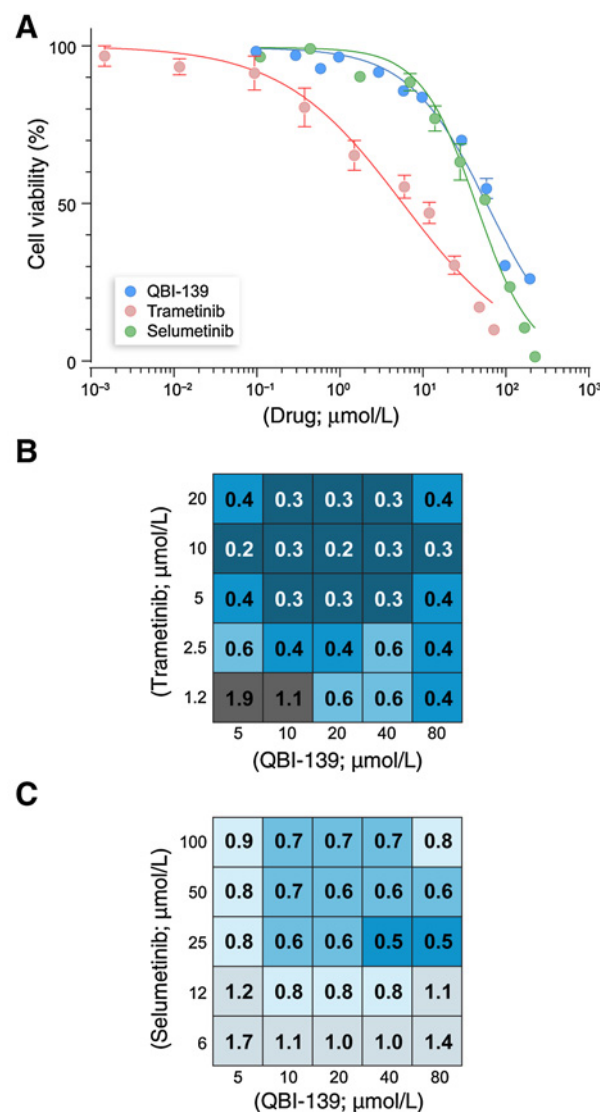


Figure 2.

Synergistic effects of ERK-pathway inhibitors and QBI-139 on the viability of human A549 lung cancer cells. **A**, Cells were incubated with a single drug (trametinib, selumetinib, or QBI-139) for 48 hours. Cell viability was measured with a tetrazolium dye-based assay for metabolic activity. EC_{50} values are listed in Table 1. **B** and **C**, Two-drug combination experiments were performed using a 5×5 matrix to interrogate 25 concentration pairs. Cells were treated with a kinase inhibitor for 1 hour at 37°C, followed by the addition of QBI-139. Cells were incubated continually for another 48 hours. Cell viability assessments for single and combination drug treatments were evaluated to identify synergistic effects based on CI. Values of CI were calculated with CalcSyn 2.0 software. $CI < 1$ (blue), $CI = 1$, and $CI > 1$ (black) indicate synergism, an additive effect, and antagonism, respectively. The combination of trametinib and QBI-139 exerts more synergism than does the combination of selumetinib and QBI-139. Values represent the mean \pm SEM ($n = 3$, biological replicates).

assessed cell viability for single-drug and two-drug combination treatments to identify synergistic effects as judged by values of the combination index (CI), which are shown in Fig. 2B and C. We observed strong synergy between MEK inhibitors and the pTrNase, and the synergistic effect of QBI-139 paired with trametinib is more favorable than with selumetinib.

A KRAS inhibitor acts synergistically with a ptRNase

MEK is activated by BRAF, and BRAF is a substrate of KRAS. We asked if an inhibitor of the upstream activator, KRAS, acts synergistically with QBI-139. The small-molecule drug ARS-853 has robust cellular inhibitory activity against the G12C variant of KRAS (33, 34) and inhibits KRAS signaling in H358 cells (KRAS^{G12C}) but not A549 cells (KRAS^{G12S}; ref. 33), both of which are human lung cancer lines. As expected, ARS-853 treatment killed H358 cells more effectively than A549 cells (Fig. 3A and B). Interestingly, QBI-139 treatment was 20-fold more cytotoxic to H358 cells compared with A549 cells (Fig. 3A and B). Combining the KRAS^{G12C}-targeted agent, ARS-853, with QBI-139 enhanced the efficacy of both agents toward H358 cells (Fig. 3C). In contrast, this combination produced an additive effect toward A549 cells (Fig. 3D). These findings suggest some sort of molecular interaction between QBI-139 and the ERK pathway.

QBI-139 exhibits greater synergy with a BRAF or MEK inhibitor than do combinations of BRAF and MEK inhibitors

Substitutions to Val600 of BRAF lead to strongly growth-promoting signals and are often found in patients with advanced melanoma. Trametinib, in combination with dabrafenib, is in clinical use for the treatment of patients with BRAF^{V600E} metastatic melanoma. Dabrafenib has robust inhibitory activity against V600E variants of BRAF (35, 36). Tumors often develop resistance to BRAF inhibitors by activating MEK and resuming growth (37–41).

We assessed the effect of kinase inhibitors in combination with QBI-139 across three BRAF^{V600E} melanoma cell lines: SK-MEL-28, A375, and Malme-3M. We observed strong synergy with dabrafenib and QBI-139, and somewhat weaker synergy with trametinib and QBI-139; whereas dabrafenib and trametinib exhibited an additive effect (Fig. 4). None of the agents

were toxic to normal skin fibroblasts at the tested doses (Supplementary Fig. S1).

RI is a substrate for kinases of the ERK pathway

No known mechanism-of-action can explain the synergism of QBI-139 with a protein kinase inhibitor. Because RI is a critical regulator of ptRNase activity in the cell (42–44), we hypothesized that RI undergoes phosphorylation in mammalian cells. Coulombic interactions make a strong contribution to the affinity of RI and ptRNases, which are highly anionic and highly cationic, respectively (22, 45–47). The addition of anionic phosphoryl groups to RI would likely enhance this Coulombic interaction.

We sought to identify a kinase that could phosphorylate RI. For guidance, we analyzed the amino-acid sequence of RI with the program NetPhos 3.1 (48, 49). The computational results indicated that RI was likely to be a substrate for ERK and RSK. Notably, this assignment is consistent with the cooperative action of QBI-139 and ERK-pathway inhibitors (Fig. 1–4).

Phosphorylation of RI enhances its interaction with ptRNases

To test for RI-phosphorylation and an increased affinity for a ptRNase, we isolated RI from mammalian cells. Specifically, we produced biotinylated RI in HEK293T cells through transient co-transfection of both a plasmid that directs the expression of RI conjugated to a biotin-acceptor-peptide (BAP) and another plasmid that directs the expression of biotin ligase (BirA), which catalyzes the condensation of biotin with a lysine residue in BAP. Assays of different ratios of Lipofectamine 3000 to plasmids revealed a 1:1 ratio as yielding the most biotinylated RI (Supplementary Fig. S2A). RI expression was found to be higher at 48 hours after transfection than at 24 or 72 hours (Supplementary Fig. S2B and S2C). Biotinylated RI was purified by column chromatography using monomeric avidin–agarose

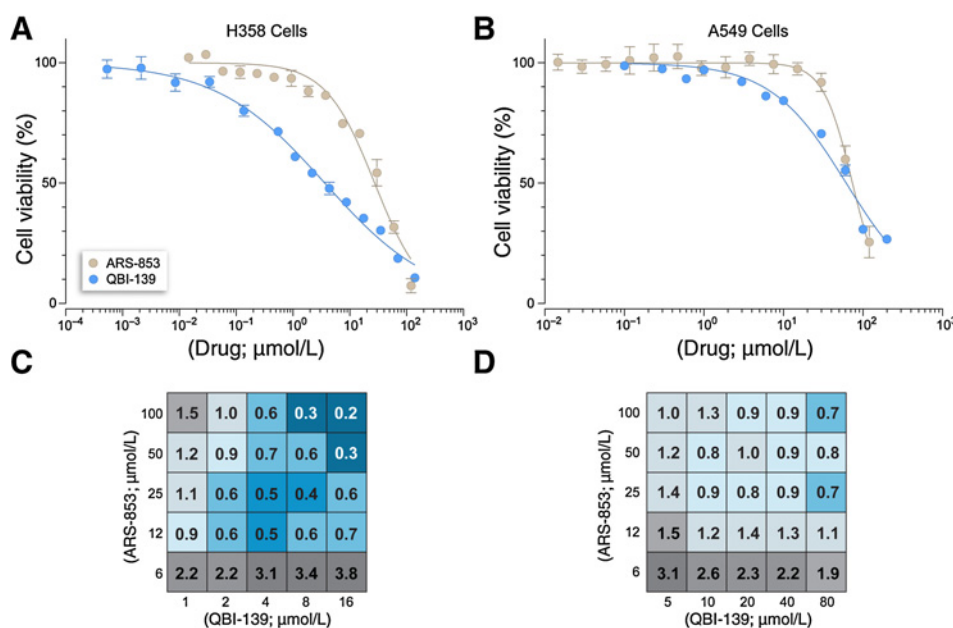


Figure 3.

Inhibition of the ERK pathway enhances the toxicity of QBI-139 for human lung cancer cells. **A**, QBI-139 is more toxic to H358 cells ($EC_{50} = 3.6 \pm 0.6 \mu\text{mol/L}$), which harbor the KRAS^{G12C} variant, than is ARS-853 ($EC_{50} = 28 \pm 4 \mu\text{mol/L}$). Values represent the mean \pm SEM ($n = 3$, biological replicates). **B**, QBI-139 and ARS-853 have indistinguishable toxicity for A549 cells ($EC_{50} = 62 \pm 7 \mu\text{mol/L}$ and $EC_{50} = 74 \pm 8 \mu\text{mol/L}$, respectively). Data for the toxicity of QBI-139 are from Fig. 2A. Values represent the mean \pm SEM ($n = 3$, biological replicates). **C** and **D**, Synergistic effects of ARS-853 and QBI-139. The combination exerts greater synergism against H358 cells than against A549 cells.

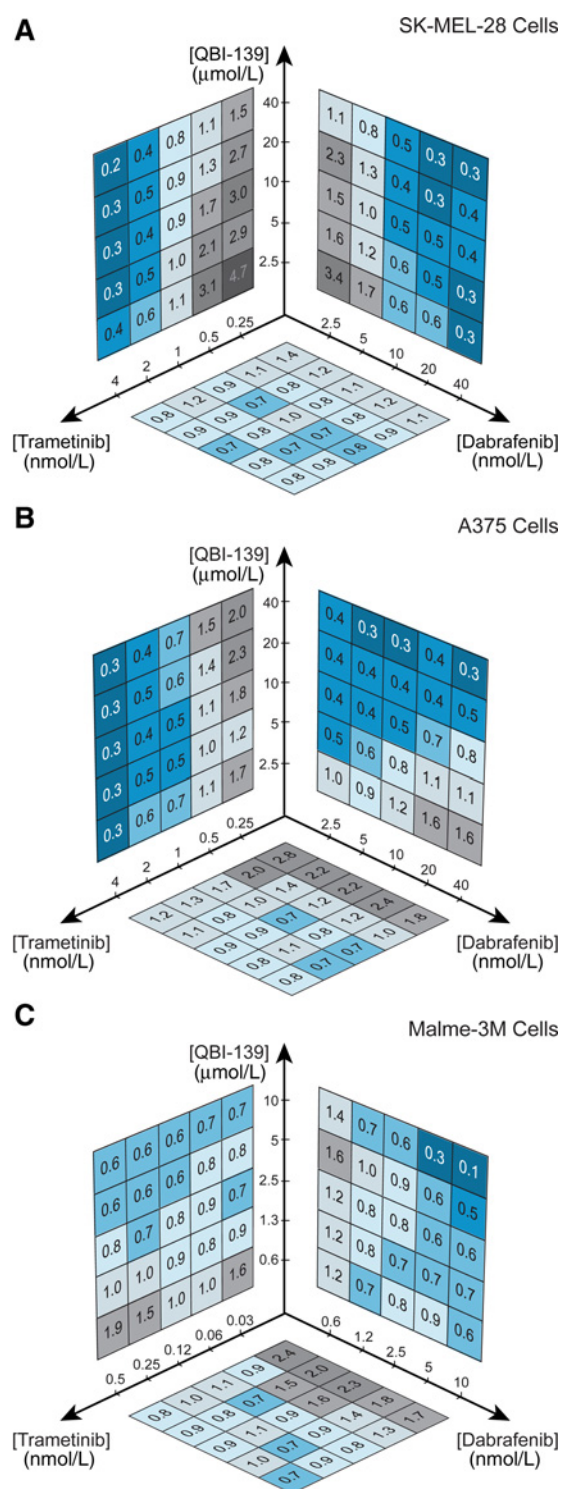


Figure 4. Synergistic effects of the combined treatment of kinase inhibitors and QBI-139 on human melanoma cells. The combination of dabrafenib and QBI-139 exerts greater synergism than does the combination of trametinib and QBI-139 across 3 different melanoma cell lines: **A**, SK-MEL-28 cells; **B**, A375 cells; and **C**, Malme-3M cells. Treatment with the two kinase inhibitors, trametinib and dabrafenib, results in additive effects. Values represent the mean ± SEM ($n = 3$, biological replicates).

and RNase A-affinity resin. Elution of biotinylated RI from the RNase A-affinity resin required 3.5 mol/L NaCl, in contrast to the 3.0 mol/L NaCl necessary to elute RI produced in *Escherichia coli* (Supplementary Fig. S2D). Elution at a higher salt concentration suggests a greater affinity of a ptRNase for mammalian-derived RI.

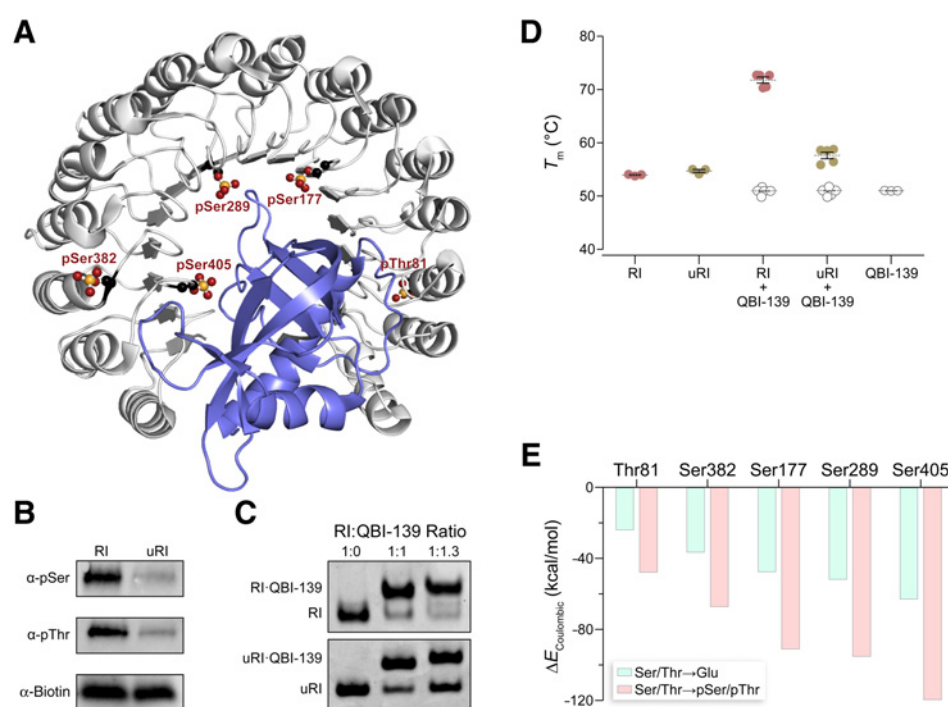
We discovered that RI is indeed phosphorylated by intracellular kinases. Incubation of *E. coli*-derived RI with HEK293T cell lysate and [γ - 32 P]ATP led to 32 P-labeled RI (Supplementary Fig. S2E). To refine this result, we isolated RI from live HEK293T cells and analyzed the protein by mass spectrometry. Phosphoryl groups were apparent on five residues: Thr81, Ser177, Ser289, Ser382, and Ser405 (Fig. 5A and Supplementary Fig. S3). Finally, we confirmed the endogenous phosphorylation of RI further by immunoblotting the isolated RI with antibodies that recognize phosphoserine (α -pSer) and phosphothreonine (α -pThr; Fig. 5B). Application of lambda protein phosphatase to the same sample produced unphosphorylated (uRI), which did not yield a signal in the immunoblot.

We interrogated the effect of RI phosphorylation using a native gel-shift assay. An equimolar or greater amount of QBI-139 was incubated with RI, and a shift in the position of RI on the gel reported on the extent of complex formation. Although QBI-139 evades unphosphorylated RI, that evasion is not complete, as uRI splits into free and ptRNase-bound populations (Fig. 5C). In contrast, phosphorylated RI exhibits near-complete binding to QBI-139. Thus, the presence of phosphoryl groups on RI enhances its interaction with a ptRNase.

The enhanced affinity of phosphorylated RI for a ptRNase was also apparent in thermal denaturation experiments. Binding to a ligand stabilizes a protein (24, 25, 50, 51). Although not changing the thermostability of RI itself, phosphorylation generates a marked increase in the thermostability of an RI-ptRNase complex (Fig. 5D). The T_m value of the phosphorylated RI-QBI-139 complex is 15°C higher than that of uRI-QBI-139, indicative of enhanced affinity and in accord with the results of the native gel-shift assay (Fig. 5C). Moreover, computational models suggest a stronger Coulombic interaction between RI and RNase 1 upon phosphorylation of RI, especially on residues closest to the RI-RNase 1 interface (Fig. 5E). Together, these data indicate a direct link between the phosphorylation of RI and an increase in its affinity for ptRNases.

Phosphorylation of RI is suppressed by inhibitors of the ERK pathway

Finally, we sought to confirm the apparent effect of kinase inhibitors on RI phosphorylation by immunoblotting. Biotinylated RI was isolated by using streptavidin-coated magnetic beads from SK-MEL-28 cells after transient transfection for 48 hours. To detect phosphorylated species, we used α -pSer or α -pThr. Strong bands for phosphorylated RI were observed when cells were treated with inhibitors of kinases that are not on the ERK pathway (Fig. 6). Those kinase inhibitors (PD 0332991, bosutinib, and crizotinib) had insignificant effects on the phosphorylation of MEK, ERK, or RSK (Fig. 6A). In contrast, cells treated with a BRAF-targeted agent, dabrafenib, produced only a weak band of phosphorylated MEK, and no detectable phosphorylation of downstream targets, including ERK, RSK, and RI. Likewise, treatment with MEK-targeted agents, trametinib or selumetinib, diminished the phosphorylation of ERK, RSK, and RI. These biochemical data provide direct evidence that kinases in the ERK pathway are

**Figure 5.**

Characterization of phosphorylated RI. **A**, Structure of the RI-RNase 1 complex (PDB entry 1z7x). Phosphorylated residues identified by mass spectrometry are modeled and depicted in ball-and-stick representation. Image was created with the program PyMOL from Schrödinger (New York, NY). **B**, Immunoblots showing that RI produced by HEK293T cells is recognized by an anti-phosphoserine antibody (α -pSer) and anti-phosphothreonine antibody (α -pThr). That recognition is eliminated upon treatment with lambda protein phosphatase (unphosphorylated RI, uRI). **C**, Non-denaturing PAGE gel showing complex formation of RI and QBI-139. Lane 1, free RI (3.0 μ mol/L); lanes 2 and 3, complex of RI (3.0 μ mol/L) with QBI-139 (4.0 μ mol/L and 3.0 μ mol/L). Proteins (in PBS) were incubated for 20 minutes before loading on the gel. **D**, Graph showing that RI and uRI have similar thermostability. The presence of QBI-139 increases the T_m value of RI by 18°C. In contrast, the presence of QBI-139 increases the T_m value of uRI by only 3°C. Individual circles represent the mean \pm SEM ($n \geq 3$, technical replicates). **E**, Graph showing energies calculated for changes in Coulombic interaction between RI and RNase 1 upon phosphorylation of RI at particular Ser/Thr residues.

indeed responsible for phosphorylating RI, in agreement with the observed synergism.

Discussion

RI is a 50-kDa cytosolic protein found in all mammalian cells (4), and is not known to undergo phosphorylation (52). Human RI is composed of 15 leucine-rich repeats that endow the protein with the shape of a horseshoe (53, 54), which is conserved in homologs (47). The cytosolic concentration of RI is approximately 4 μ mol/L (42). This relatively high concentration, coupled with the ubiquitous expression of its mRNA in mammalian tissues, is consistent with an important role.

RI is known to act as a "sentry" that protects mammalian cells from ptRNases (42–44). These ribonucleases are secretory (~ 0.5 μ g/mL in human blood and serum; ref. 24) but can enter cells via endocytosis (55, 56). A fraction of the protein escapes from endosomes into the cytosol but is then inhibited by RI (55, 56). A ptRNase that is resistant to RI can degrade cellular RNAs, resulting in apoptosis (5, 6). Such RI-evasive homologs and variants have shown promise as cancer chemotherapeutic agents (57, 58).

RI-ptRNase complexes have K_d values in the sub-femtomolar range (4, 6), making the RI-ptRNase interaction the tightest known between biomolecules. The RI-ptRNase complex is stabilized by favorable Coulombic interactions, as RI is highly anionic

and ptRNases are highly cationic (22, 45–47). To date, all detailed structure–function analyses of RI have been performed on protein produced by heterologous expression in *E. coli*.

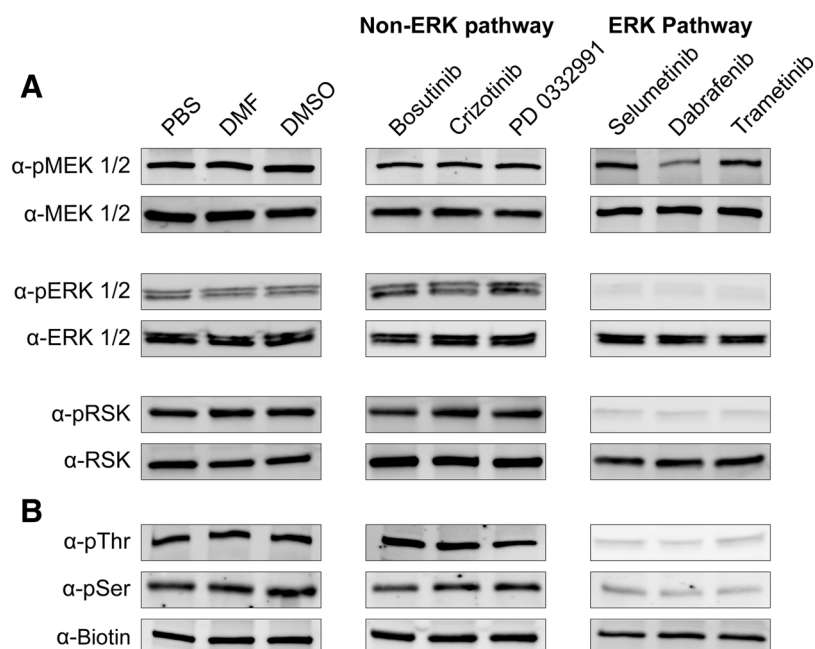
Apparently, femtomolar affinity is not enough. We discovered that five residues of RI are phosphorylated by kinases in the ERK pathway (Fig. 5A and B), and that phosphorylation increases the affinity of RI for a ptRNase (Fig. 5C and D). Computational models suggest that three of the nascent phosphoryl groups (*i.e.*, those on Ser177, Ser289, and Ser405) are especially favorable for interaction with bound RNase 1 (Fig. 5E). These three sites have been conserved during mammalian evolution (Supplementary Fig. S4).

The phosphoryl group on Ser405 merits special consideration. ptRNases have four well-defined enzymic subsites that bind to phosphoryl groups in an RNA substrate (59–61). A phosphoryl group on Ser405 is proximal to each of those subsites in an RI-ptRNase complex (Supplementary Fig. S5). In other words, a post-translational modification installs a phosphoryl group in the inhibitor of an enzyme in a location that recapitulates the phosphoryl groups in the substrate of that enzyme.

RI also inhibits an atypical ptRNase, angiogenin (ANG), which is a potent inducer of neovascularization (62). Whereas other ptRNases function in the extracellular space or cytosol, ANG acts in the nucleolus (63, 64). Gain- and loss-of-function experiments have elucidated the roles of RI in regulating angiogenesis through direct interaction with ANG (65–69). Phosphorylation enables

Figure 6.

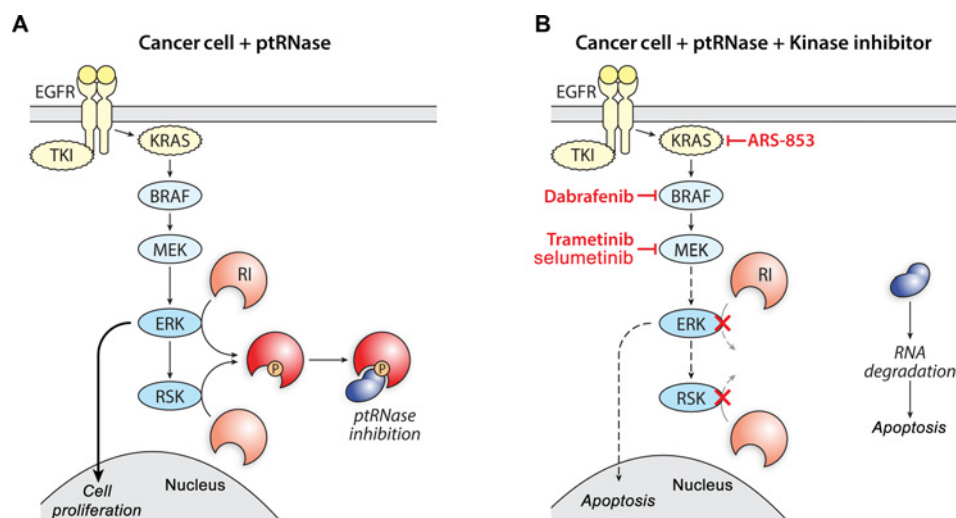
Immunoblots showing that inhibition of the ERK pathway diminishes the phosphorylation of RI in SK-MEL-28 cells. Cells transfected to produce biotinylated RI were treated with bosutinib (5 μ mol/L), crizotinib (2 μ mol/L), PD 0332991 (2 μ mol/L), selumetinib (10 nmol/L), dabrafenib (10 nmol/L), or trametinib (1 nmol/L) for 24 hours. **A**, Treatment with inhibitors of non-ERK pathway kinases has no effect on the phosphorylation of MEK, ERK, or RSK in cell lysates. Treatment with dabrafenib reduces the phosphorylation of MEK (α -pMEK 1/2 lane) as well as that of ERK and RSK (α -pERK 1/2, and α -pRSK lanes). Treatment with selumetinib and trametinib reduces the phosphorylation of ERK and RSK. **B**, Treatment with inhibitors of non-ERK pathway kinases has no effect on the phosphorylation of biotinylated RI, which was captured by using streptavidin-coated magnetic beads. Inhibition of ERK-pathway kinases diminishes phosphorylation of RI (α -pThr and α -pSer lanes).



ANG to evade cytosolic RI on its route to the nucleolus (23). Appending phosphoryl groups to RI generates repulsive Coulombic interactions that are likely to diminish its affinity for ANG even further. In particular, Ser289 of RI is proximal to phosphorylated Ser87 of ANG in the RI-ANG complex (Supplementary Fig. S6A), and Ser405 of RI is close to Asp41 of ANG (Supplementary Fig. S6B). Notably, Ser87 is not known to be phosphorylated in other ptRNases, and Asp41 is nearly always replaced with a proline residue in homologs (70). Thus, phosphorylation might enable

RI to discriminate between homologous human proteins—enhancing affinity for RNase 1 but diminishing affinity for ANG.

Whereas the phosphorylation of Ser177, Ser289, and Ser405 of RI affects its affinity for ptRNases, the phosphorylation of Thr81 and Ser382 could affect the oxidative stability of RI. Both of these residues are proximal to cysteine residues in the folded protein (Supplementary Fig. S7A and S7B). RI is vulnerable to cooperative oxidation that is detrimental to its structure and function, and leads to proteolysis (71, 72). A sulfhydryl group

**Figure 7.**

Putative mechanism of synergy between an ERK-pathway inhibitor and a ptRNase. The binding of growth factors to extracellular receptors activates Ras, which in turn activates the protein kinase activity of Raf kinase (82). Raf kinase catalyzes the phosphorylation of MEK, and MEK catalyzes the phosphorylation of ERK (83). ERK has more than 400 substrates, including p90 ribosomal S6 kinase-1 (RSK; ref. 84), and its kinase activity regulates gene expression related to cell growth and proliferation. ERK and RSK catalyze the phosphorylation of RI, which strengthens the interaction of RI with an invading ptRNase (**A**). Treatment with a kinase inhibitor (e.g., ARS-853, dabrafenib, trametinib, or selumetinib) diminishes RI phosphorylation, which unleashes a larger portion of the invading ptRNase to manifest cytotoxic ribonucleolytic activity (**B**).

is oxidized much more readily upon deprotonation to a thiolate (73), which is anionic. Accordingly, cysteine residues in an anionic environment are likely to be resistant to oxidation (Supplementary Fig. S7C), and the phosphorylation of RI could confer such resistance.

RI is phosphorylated by kinases of the ERK pathway. The ERK pathway is deregulated in a third of all human cancers (74–76). Small-molecule inhibitors that target components of the ERK cascade can halt the propagation of growth stimuli and be effective anticancer agents (77–79). The development of resistance, however, limits the effectiveness of these inhibitors (18). For example, trametinib and dabrafenib were approved in 2013 as single agents for the treatment of BRAF^{V600E} mutation-positive unresectable or metastatic melanoma (36, 80, 81). Many patients, however, develop resistance to these drugs within a few months (18, 19). In 2014, the FDA-granted approval for a combination therapy of trametinib and dabrafenib, with the hope of combatting resistance (38, 39, 41). We find that coupling either trametinib or dabrafenib with QBI-139, a cytotoxic ptRNase, provides much more synergistic toxicity for melanoma cells than does coupling trametinib with dabrafenib (Fig. 5). This synergism between a kinase inhibitor and QBI-139 is consistent with underlying mechanisms of action (Fig. 7) as well as rational strategies for the beneficial combination of drugs (10, 11). Hence, the discovery of RI phosphorylation could have clinical implications, including to cancer patients suffering from "addiction" to drugs that target the ERK pathway (40).

References

- Ledoux L, Baltus E. Action de la ribonucléase sur les cellules du carcinome d'Ehrlich. *Experientia* 1954;10:500–1.
- Ledoux L. Action of ribonuclease on two solid tumours *in vivo*. *Nature* 1955;176:36–7.
- Ledoux L. Action of ribonuclease on certain ascites tumours. *Nature* 1955;175:258–9.
- Dickson KA, Haigis MC, Raines RT. Ribonuclease inhibitor: structure and function. *Prog Nucleic Acid Res Mol Biol* 2005;80:349–74.
- Rutkowski TJ, Raines RT. Evasion of ribonuclease inhibitor as a determinant of ribonuclease cytotoxicity. *Curr Pharm Biotechnol* 2008;9:185–9.
- Lomax JE, Eller CH, Raines RT. Rational design and evaluation of mammalian ribonuclease cytotoxins. *Methods Enzymol* 2012;502:273–90.
- Eller CH, Chao T-Y, Singarapu KK, Ouerfelli O, Yang G, Markley JL, et al. Human cancer antigen Globo H is a cell-surface ligand for human ribonuclease 1. *ACS Cent Sci* 2015;1:181–90.
- Strong LE, Kink JA, Pensinger D, Mei B, Shahan M, Raines RT. Efficacy of ribonuclease QBI-139 in combination with standard of care therapies. *Cancer Res* 2012;72(Suppl. 1):1838.
- Strong LE, Kink JA, Mei B, Shahan MN, Raines RT. First in human phase I clinical trial of QBI-139, a human ribonuclease variant, in solid tumors. *J Clin Oncol* 2012;30(Suppl.):TPS3113.
- Dancey JE, Chen HX. Strategies for optimizing combinations of molecularly targeted anticancer agents. *Nat Rev Drug Discov* 2006;5:649–59.
- Lopez JS, Banerji U. Combine and conquer: Challenges for targeted therapy combinations in early phase trials. *Nat Rev Clin Oncol* 2016;14:57–66.
- Bozic I, Reiter JG, Allen B, Antal T, Chatterjee K, Shah P, et al. Evolutionary dynamics of cancer in response to targeted combination therapy. *eLife* 2013;2:e00747.
- Zhou A, Paranjape J, Brown TL, Nie H, Naik S, Dong B, et al. Interferon action and apoptosis are defective in mice devoid of 2',5'-oligoadenylate-dependent RNase L. *EMBO J* 1997;16:6355–63.
- Cohen P. The regulation of protein function by multisite phosphorylation—a 25 year update. *Trends Biochem Sci* 2000;25:596–601.
- Johnson LN. The regulation of protein phosphorylation. *Biochem Soc Trans* 2009;38:627–41.
- Shaul YD, Seger R. The MEK/ERK cascade: From signaling specificity to diverse functions. *Biochim Biophys Acta* 2007;1773:1213–26.
- Samatar AA, Poulikakos PI. Targeting RAS-ERK signalling in cancer: Promises and challenges. *Nat Rev Drug Discov* 2014;13:928–42.
- McCubrey JA, Steelman LS, Chappell WH, Abrams SL, Wong EWT, Chang F, et al. Roles of the Raf/MEK/ERK pathway in cell growth, malignant transformation and drug resistance. *Biochim Biophys Acta* 2007;1773:1263–84.
- Yu Z, Ye S, Hu G, Lv M, Tu Z, Zhou K, et al. The RAF-MEK-ERK pathway: targeting ERK to overcome obstacles to effective cancer therapy. *Fut Med Chem* 2015;7:269–89.
- Cory AH, Owen TC, Barltrop JA, Cory JG. Use of an aqueous soluble tetrazolium/formazan assay for cell growth assays in culture. *Cancer Commun* 1991;3:207–12.
- Gibson DG, Young L, Chuang R-Y, Venter JC, Hutchinson CA III, Smith HO. Enzymatic assembly of DNA molecules up to several hundred kilobases. *Nat Methods* 2009;6:343–5.
- Johnson RJ, McCoy JG, Bingman CA, Phillips GN Jr, Raines RT. Inhibition of human pancreatic ribonuclease by the human ribonuclease inhibitor protein. *J Mol Biol* 2007;367:434–49.
- Hoang TT, Raines RT. Molecular basis for the autonomous promotion of cell proliferation by angiogenin. *Nucleic Acids Res* 2017;45:818–31.
- Lomax JE, Eller CH, Raines RT. Comparative functional analysis of ribonuclease 1 homologs: Molecular insights into evolving vertebrate physiology. *Biochem J* 2017;474:2219–33.
- Niesen FH, Berglund H, Vedadi M. The use of differential scanning fluorimetry to detect ligand interactions that promote protein stability. *Nat Protoc* 2007;2:2212–21.
- Word JM, Lovell SC, Richardson JS, Richardson DC. Asparagine and glutamine: Using hydrogen atom contacts in the choice of side-chain amide orientation. *J Mol Biol* 1999;285:1735–47.

Disclosure of Potential Conflicts of Interest

R.T. Raines has ownership interest (including stock, patents, etc.) in Quintessence Biosciences, Inc. No potential conflicts of interest were disclosed by the other authors.

Authors' Contributions

Conception and design: T.T. Hoang, R.T. Raines

Development of methodology: T.T. Hoang, I.C. Tanrikulu, Q.A. Vatland

Acquisition of data (provided animals, acquired and managed patients, provided facilities, etc.): T.T. Hoang, I.C. Tanrikulu, Q.A. Vatland, T.M. Hoang

Analysis and interpretation of data (e.g., statistical analysis, biostatistics, computational analysis): T.T. Hoang, I.C. Tanrikulu, T.M. Hoang, R.T. Raines
Writing, review, and/or revision of the manuscript: T.T. Hoang, I.C. Tanrikulu, R.T. Raines

Administrative, technical, or material support (i.e., reporting or organizing data, constructing databases): T.T. Hoang, T.M. Hoang, R.T. Raines

Study supervision: T.T. Hoang, R.T. Raines

Acknowledgments

We are grateful to Dr. Bryan D. Smith (Deciphera Pharmaceuticals) for helpful comments on the article. T.T. Hoang was supported by Molecular Biosciences Training Grant T32 GM007215 (NIH) to the University of Wisconsin–Madison. This work was supported by Grant R01 CA073808 (NIH; to R.T. Raines).

The costs of publication of this article were defrayed in part by the payment of page charges. This article must therefore be hereby marked *advertisement* in accordance with 18 U.S.C. Section 1734 solely to indicate this fact.

Received July 1, 2018; revised August 15, 2018; accepted September 27, 2018; published first October 3, 2018.

27. Mayo SL, Olafson BD, Goddard WA III. DREIDING: A generic force field for molecular simulations. *J Phys Chem* 1990;94:8897–909.
28. Lim K-T, Brunett S, Iotov M, McClurg RB, Vaidehi N, Dasgupta S, et al. Molecular dynamics for very large systems on massively parallel computers: The MPSim program. *J Comput Chem* 1997;18: 501–21.
29. Kam VWT, Goddard WA III. Flat-bottom strategy for improved accuracy in protein side-chain placements. *J Chem Theor Comput* 2008;4: 2160–9.
30. Boschelli DH, Ye F, Wang YD, Dutia M, Johnson SL, Wu B, et al. Optimization of 4-phenylamino-3-quinolinecarbonitriles as potent inhibitors of Src kinase activity. *J Med Chem* 2001;44:3965–77.
31. Fry DW, Harvey PJ, Keller PR, Elliott WL, Meade M, Trachet E, et al. Specific inhibition of cyclin-dependent kinase 4/6 by PD 0332991 and associated antitumor activity in human tumor xenografts. *Mol Cancer Ther* 2004; 3:1427–38.
32. Zou HY, Li Q, Lee JH, Arango ME, McDonnell SR, Yamazaki S, et al. An orally available small-molecule inhibitor of c-Met, PF-2341066, exhibits cytoreductive antitumor efficacy through antiproliferative and antiangiogenic mechanisms. *Cancer Res* 2007;67:4408–17.
33. Patricelli MP, Janes MR, Li L-S, Hansen R, Peters U, Kessler LV, et al. Selective inhibition of oncogenic KRAS output with small molecules targeting the inactive state. *Cancer Discov* 2016;6:316–29.
34. Lito P, Solomon M, Li L-S, Hansen R, Rosen N. Allele-specific inhibitors inactivate mutant KRAS G12C by a trapping mechanism. *Science* 2016;351:604–8.
35. Kefford R, Arkenau H, Brown MP, Millward M, Infante JR, Long GV, et al. Phase I/II study of GSK2118436, a selective inhibitor of oncogenic mutant BRAF kinase, in patients with metastatic melanoma and other solid tumors. *J Clin Oncol* 2010;28 Suppl.:8503.
36. King AJ, Amone MR, Bleam MR, Moss KG, Yang J, Fedorowicz KE, et al. Dabrafenib; preclinical characterization, increased efficacy when combined with trametinib, while BRAF/MEK tool combination reduced skin lesions. *PLoS ONE* 2013;8:e67583.
37. Greger JG, Eastman SD, Zhang V, Bleam MR, Hughes AM, Smiehemann KN, et al. Combinations of BRAF, MEK, and PI3K/mTOR inhibitors overcome acquired resistance to the BRAF inhibitor GSK2118436 dabrafenib, mediated by NRAS or MEK mutations. *Mol Cancer Ther* 2012;11:909–20.
38. McArthur G. Combination therapies to inhibit the RAF/MEK/ERK pathway in melanoma: We are not done yet. *Front Oncol* 2015;5:161.
39. Long GV, Stroyakovskiy D, Gogas H, Levchenko E, de Braud F, Larkin J, et al. Dabrafenib and trametinib versus dabrafenib and placebo for Val600 BRAF-mutant melanoma: A multicentre, double-blind, phase 3 randomised controlled trial. *Lancet* 2015;386:444–51.
40. Kong A, Kuilman T, Shahrahi A, Boshuizen J, Kemper K, Song J-Y, et al. Cancer drug addition is related by an ERK2-dependent phenotype switch. *Nature* 2017;550:270–4.
41. Long GV, Hauschild A, Santinami M, Atkinson V, Mandalà M, Chiarion-Sileni V, et al. Adjuvant dabrafenib plus trametinib in stage III BRAF-mutated melanoma. *N Eng J Med* 2017;1813–23.
42. Haigis MC, Kurten EL, Raines RT. Ribonuclease inhibitor as an intracellular sentry. *Nucleic Acids Res* 2003;31:1024–32.
43. Thomas SP, Kim E, Kim J-S, Raines RT. Knockout of the ribonuclease inhibitor gene leaves human cells vulnerable to secretory ribonucleases. *Biochemistry* 2016;55:6359–62.
44. Thomas SP, Hoang TT, Ressler VT, Raines RT. Human angiogenin is a potent cytotoxin in the absence of ribonuclease inhibitor. *RNA* 2018;24:1018–27.
45. Kobe B, Deisenhofer J. A structural basis of the interactions between leucine-rich repeats and protein ligands. *Nature* 1995;374:183–6.
46. Papageorgiou AC, Shapiro R, Acharya KR. Molecular recognition of human angiogenin by placental ribonuclease inhibitor—an X-ray crystallographic study at 2.0 Å resolution. *EMBO J* 1997;16:5162–77.
47. Lomax JE, Bianchetti CM, Chang A, Phillips GN Jr, Fox BG, Raines RT. Functional evolution of ribonuclease inhibitor: Insights from birds and reptiles. *J Mol Biol* 2014;26:3041–56.
48. Blom N, Gammeltoft S, Brunak S. Sequence and structure-based prediction of eukaryotic protein phosphorylation sites. *J Mol Biol* 1999; 294:1351–62.
49. Blom N, Sicheritz-Pontén T, Gupta R, Gammeltoft S, Brunak S. Prediction of post-translational glycosylation and phosphorylation of proteins from the amino acid sequence. *Proteomics* 2004;4: 1633–49.
50. Klink TA, Vicentini AM, Hofsteenge J, Raines RT. High-level soluble production and characterization of porcine ribonuclease inhibitor. *Protein Expression Purif* 2001;22:174–9.
51. Park C, Marqusee S. Pulse proteolysis: A simple method for quantitative determination of protein stability and ligand binding. *Nat Methods* 2005;2:207–12.
52. Vlastaridis P, Kyriakidou P, Chaliotis A, Van de Peer Y, Oliver SG, Amoutzias GD. Estimating the total number of phosphoproteins and phosphorylation sites in eukaryotic proteomes. *GigaScience* 2017; 6:1–11.
53. Kobe B, Deisenhofer J. Crystal structure of porcine ribonuclease inhibitor, a protein with leucine-rich repeats. *Nature* 1993;366:751–6.
54. Kajava AV. Structural diversity of leucine-rich repeat proteins. *J Mol Biol* 1998;277:519–27.
55. Chao T-Y, Lavis LD, Raines RT. Cellular uptake of ribonuclease A relies on anionic glycans. *Biochemistry* 2010;49:10666–73.
56. Chao T-Y, Raines RT. Mechanism of ribonuclease A endocytosis: Analogies to cell-penetrating peptides. *Biochemistry* 2011;50:8374–82.
57. Ardel W, Ardel B, Darzynkiewicz Z. Ribonucleases as potential modalities in anticancer therapy. *Eur J Pharmacol* 2009;625:181–9.
58. Fang EF, Ng TB. Ribonucleases of different origins with a wide spectrum of medicinal applications. *Biochim Biophys Acta* 2011; 1815:65–74.
59. Nogués MV, Moussaoui M, Boix E, Vilanova M, Ribó M, Cuchillo CM. The contribution of noncatalytic phosphate-binding subsites to the mechanism of bovine pancreatic ribonuclease A. *Cell Mol Life Sci* 1998;54: 766–74.
60. Fisher BM, Grilley JE, Raines RT. A new remote subsite in ribonuclease A. *J Biol Chem* 1998;273:34134–8.
61. Thiagarajan N, Smith BD, Raines RT, Acharya KR. Functional and structural analyses of N-acetylsulfonamide-linked dinucleoside inhibitors of bovine pancreatic ribonuclease. *FEBS J* 2011;278:541–9.
62. Fett JW, Strydom DJ, Lobb RR, Alderman EM, Bethune JL, Riordan JF, et al. Isolation and characterization of angiogenin, an angiogenic protein from human carcinoma cells. *Biochemistry* 1985;24:5480–6.
63. Moroiu J, Riordan JF. Nuclear translocation of angiogenin in proliferating endothelial cells is essential to its angiogenic activity. *Proc Natl Acad Sci U S A* 1994;91:1677–81.
64. Xu Z-p, Tsuji T, Riordan JF, Hu G-f. The nuclear function of angiogenin in endothelial cells is related to rRNA production. *Biochem Biophys Res Commun* 2002;294:287–92.
65. Shapiro R, Vallee BL. Human placental ribonuclease inhibitor abolishes both angiogenic and ribonucleolytic activities of angiogenin. *Proc Natl Acad Sci U S A* 1987;84:2238–41.
66. Pizzo E, D'Alessio G. The success of the RNase scaffold in the advance of biosciences and in evolution. *Gene* 2007;406:8–12.
67. Dickson KA, Kang D-K, Kwon YS, Kim JC, Leland PA, Kim B-M, et al. Ribonuclease inhibitor regulates neovascularization by human angiogenin. *Biochemistry* 2009;48:3804–6.
68. Li L, pan X-Y, Shu J, Jiang R, Zhou Y-J, Chen J-X. Ribonuclease inhibitor up-regulation inhibits the growth and induces apoptosis in murine melanoma cells through repression of angiogenin and ILK/PI3K/AKT signaling pathway. *Biochimie* 2014;103:89–100.
69. Lyons SM, Fay MM, Akiyama Y, Anderson PJ, Ivanov P. RNA biology of angiogenin: Current state and perspectives. *RNA Biol* 2017;14: 171–8.
70. Beintema JJ, Schüller C, Irie M, Carsana A. Molecular evolution of the ribonuclease superfamily. *Prog Biophys Molec Biol* 1988;51: 165–92.
71. Fominaya JM, Hofsteenge J. Inactivation of ribonuclease inhibitor by thiol–disulfide exchange. *J Biol Chem* 1992;267:24655–60.
72. Ferreras M, Gavilanes JG, López-Otín C, García-Segura JM. Thiol–disulfide exchange of ribonuclease inhibitor bound to ribonuclease A. *J Biol Chem* 1995;270:28570–8.
73. Poole LB. The basics of thiols and cysteines in redox biology and chemistry. *Free Radic Biol Med* 2015;80:148–57.

Hoang et al.

74. Dunn KL, Espino PS, Drohic B, He S, Davie JR. The Ras–MAPK signal transduction pathway, cancer and chromatin remodeling. *Biochem Cell Biol* 2005;83:1–14.
75. Torii S, Yamamoto T, Tsuchiya Y, Nishida E. ERK MAP kinase in G cell cycle progression and cancer. *Cancer Sci* 2006;97:697–702.
76. Dhillon AS, Hagan S, Rath O, Kolch W. MAP kinase signalling pathways in cancer. *Oncogene* 2007;26:3279–90.
77. Knight ZA, Shokat KM. Features of selective kinase inhibitors. *Chem Biol* 2005;12:621–37.
78. Roberts PJ, Der CJ. Targeting the Raf–MEK–ERK mitogen-activated protein kinase cascade for the treatment of cancer. *Oncogene* 2007;26:3291–310.
79. Knight ZA, Lin H, Shokat KM. Targeting the cancer kinome through polypharmacology. *Nat Rev Cancer* 2010;10:130–7.
80. Lugowska I, Kosela-Paterczyk H, Kozak K, Rutkowski P. Trametinib: A MEK inhibitor for management of metastatic melanoma. *Onco Targets Ther* 2015;8:2251–9.
81. Wellbrock C, Arozarena I. The complexity of the ERK/MAP-kinase pathway and the treatment of melanoma skin cancer. *Front Cell Dev Biol* 2016;4:33.
82. Ostrem JM, Shokat KM. Direct small-molecule inhibitors of KRAS: From structural insights to mechanism-based design. *Nat Rev Drug Discov* 2016;15:771–85.
83. Roskoski R Jr. MEK1/2 dual-specificity protein kinases: Structure and regulation. *Biochem Biophys Res Commun* 2012;417:5–10.
84. Anjum R, Blenis J. The RSK family of kinases: Emerging roles in cellular signalling. *Nat Rev Mol Cell Biol* 2008;9:747–58.

Molecular Cancer Therapeutics

A Human Ribonuclease Variant and ERK-Pathway Inhibitors Exhibit Highly Synergistic Toxicity for Cancer Cells

Trish T. Hoang, I. Caglar Tanrikulu, Quinn A. Vatland, et al.

Mol Cancer Ther 2018;17:2622-2632. Published OnlineFirst October 3, 2018.

Updated version Access the most recent version of this article at:
doi:[10.1158/1535-7163.MCT-18-0724](https://doi.org/10.1158/1535-7163.MCT-18-0724)

Supplementary Material Access the most recent supplemental material at:
<http://mct.aacrjournals.org/content/suppl/2018/10/03/1535-7163.MCT-18-0724.DC1>

Cited articles This article cites 83 articles, 14 of which you can access for free at:
<http://mct.aacrjournals.org/content/17/12/2622.full#ref-list-1>

E-mail alerts [Sign up to receive free email-alerts](#) related to this article or journal.

Reprints and Subscriptions To order reprints of this article or to subscribe to the journal, contact the AACR Publications Department at pubs@aacr.org.

Permissions To request permission to re-use all or part of this article, use this link
<http://mct.aacrjournals.org/content/17/12/2622>.
Click on "Request Permissions" which will take you to the Copyright Clearance Center's (CCC) Rightslink site.